Yu Liu, Guangqiang Li*, Li Wang and Zhao Zhang

Effect of the Tundish Gunning Materials on the Steel Cleanliness

DOI 10.1515/htmp-2016-0137
Received June 29, 2016; accepted January 26, 2017

Abstract: To clarify the interaction mechanism between distinct tundish gunning materials (GM) and liquid steel, two kinds of gunning materials, namely MgO, Al_2O_3 GM, were tested. SEM, EDS, XRD and chemical analysis were carried out for steel and GM to investigate the change of chemical composition of steel in contact with GM and the interface microstructure between steel and GM after high temperature holding experiments. The steel cleanliness in terms of inclusion number density, size and size distribution was evaluated. It was found that the reducible component, low-melting-point phases and the pores in GM were passageway for steel penetration. The Al_2O_3 GM was less prone to steel penetration due to its poor wetting and the dense transition layer. MgO GM provided more oxygen and showed a stronger oxidizing capacity due to its higher content of reducible oxides (10.5 wt.% SiO_2 + 2 wt.% Fe_2O_3). The use of Al_2O_3 GM resulted in an improved steel cleanliness and consequently could be a promising refractory in the tundish lining.

Keywords: tundish, gunning materials, interaction, steel, cleanliness

Introduction

Refractories are the most important materials used in ironmaking and steelmaking processes. Over 60% of refractory products are consumed by the iron-making and steel-making industries [1]. Interactions between steel and refractory materials are of fundamental importance for steelmaking industry [2]. Most work on interaction between refractory materials and molten steel and its influence on steel cleanliness concentrated on the main types of refractory which have a prolonged exposure time to molten steel in integrated steelmaking vessels, such as for the converter or ladle bricks [2–7]. Continuous casting is the last process where steel solidifies from liquid to solid in steelmaking processes. Tundish, as the final vessel in contact with molten steel before solidifying, provides the last opportunity to optimize the steel cleanliness and is therefore of significant importance for steel quality control [8]. However, it could also introduce exogenous inclusions through refractory erosion, slag entrapment, and steel reoxidation [2, 9, 10], contaminating molten steel and degrading steel cleanliness [8].

In order to reduce the wear of tundish refractory and the reoxidation of molten steel, gunning materials (GM) are commonly used in the inner surface layer of tundish as a dispensable protective layer between the main tundish refractory and the molten steel inside tundish. Although gunning materials is in contact with steel for 16 to 24 hours, it affects the steel cleanliness due to its direct contact with molten steel after the refining stage. Currently, the MgO GM is widely used and studied. For instance, Mantovani et al. investigated the interaction between MgO-based gunning materials and an Al-killed steel with respect to steel cleanliness [9]. They identified four major interactions at the refractory/steel interface, i. e. steel infiltration into gunning material, formation of an oxidized layer and formation of many particles in the steel near to the steel/refractory interface. They also found that the $2MgO{\cdot}SiO_2$ in gunning material reacted with the dissolved Al in molten steel to form a spinel layer at the interface. The Al_2O_3 GM is relative less used and studied. Pengcheng Yan et al. investigated the interaction between Al_2O_3 GM and an Ti-killed ultra-low carbon steel [2]. They found the Al_2O_3 GM was less prone to steel infiltration than MgO GM. However, the phase changes of Al_2O_3 GM after interaction were not studied. Several groups [8, 9, 11, 12] also confirmed that FeO and MnO impurities in refractory materials contribute to steel reoxidation and result in steel contamination by introducing exogenous inclusions. SiO_2 in refractory materials

***Corresponding author: Guangqiang Li,** The State Key Laboratory of Refractories and Metallurgy, Wuhan University of Science and Technology, Wuhan 430081, China; Key Laboratory for Ferrous Metallurgy and Resources Utilization of Ministry of Education, Wuhan University of Science and Technology, Wuhan 430081, China; Collaborative Innovation Center of Steel Technology, University of Science and Technology Beijing, Beijing 100083, China, E-mail: liguangqiang@wust.edu.cn
Yu Liu, The State Key Laboratory of Refractories and Metallurgy, Wuhan University of Science and Technology, Wuhan 430081, China
Li Wang, Zhao Zhang, Key Laboratory for Ferrous Metallurgy and Resources Utilization of Ministry of Education, Wuhan University of Science and Technology, Wuhan 430081, China

could also lead to severe reoxidation of molten steel [2, 11]. Higher contents of reducible compounds in refractory materials considerably increase the total oxygen (T. O) content in the molten steel and lead to steel cleanliness degradation [11, 12]. The interaction between refractory and slag has been widely investigated [13–17]. The reactions between the infiltrating slag and the refractory phases could slow down or even prevent further infiltration either by changing the liquid composition (making it more viscous) [18] or by the formation of new phases [19], blocking the pores [15] and making the refractory more denser. Literatures focusing on quantitative investigations on the interaction mechanisms, phase changes, Al_2O_3 GM and on the resulting steel cleanliness, which are essential for the application of gunning material selection and steel quality, however are relatively less. Based on this instance, our interest lies in whether a new dense phase will form during the interaction between steel and gunning materials, which could prevent the further penetration of molten steel and steel contamination.

In the present work, two types of gunning materials, namely MgO, Al_2O_3 GM, were tested. The interactions between gunning materials and liquid steel, including chemical reactions, steel penetration, refractory corrosion, the phase changes and the oxidizing capacity of gunning materials, were investigated. The effect of gunning materials on the composition and inclusion (size, number density and size distribution) of steel was studied as well.

Experiment

Preparation of steel

Al-killed ultra-low carbon and nitrogen steel was sampled at a steel plant after the ladle refining process and used in present experiment. Table 1 shows the chemical composition of the steel measured with inductively coupled plasma-atomic emission spectroscopy (ICP-AES), C-S analyzer (model: CS-8800), and Oxygen and Nitrogen Analyzer (model: LECO-TC500). This steel grade is easily reoxidized during the continuous casting process due to its high dissolved Al (394 ppm) and Ti (667 ppm).

Table 1: Chemical composition of steel used for present experiment (mass %).

C	Si	Mn	P	S	Als	Ti	Mg	N
0.0030	0.0130	0.0770	0.0120	0.0080	0.0394	0.0667	0.0044	0.0024

Preparation of gunning materials

Two types of MgO and Al_2O_3 GM were tested. The chemical compositions are listed in Table 2. The MgO GM contains a higher content of reducible components (10.5 wt.% SiO_2 and 2 wt.% Fe_2O_3). An alumina crucible (OD = 50 mm) was coated with a layer of gunning material (thickness of gunning materials layer: 7 mm) inside (Figure 2(a)). The density of MgO and Al_2O_3 GM is about 3433 and 3496 kg/m^3, respectively. The contact area between GM and 200 g molten steel is about 25.92 cm^2.

Table 2: Chemical composition of gunning materials (mass %).

NO.	Type	MgO	CaO	SiO_2	Al_2O_3	Fe_2O_3
I	MgO	78	6.1	10.5	3.6	2
II	Al_2O_3		1.3	3.3	93.4	2

Interaction test

Tests were performed in a vertical tube furnace with $LaCrO_3$ bars as heating elements at 1823 K (1550 °C) under Ar atmospheres. The experimental set-up and procedure are shown in Figure 1. Argon (99.999 vol % purity) was blown into the furnace with a flow rate of 3.4×10^{-6} m^3/s. The alumina crucible was placed in a graphite crucible (ID = 55 mm). Around 200 g steel was charged into the crucible and melted in the furnace. Four steel samples were taken by sucking with quartz tube (ID = 4 mm) from the position closing to the bottom center of molten steel in crucible. Because the volume of the molten steel is not large, the sample taken is representative for inclusion and composition analysis. The first sample was obtained just after the melting and temperature stabilization (30 min for stabilization). The second, third and fourth one were taken at 60 min, 90 min and 120 min, respectively. A small volume of steel (around 5 g) was sucked into the quartz tube, subsequently placed into the cold quenching water for 1 min where it solidified. After 2 hours of holding, the furnace was cooled to room temperature. The crucible was then taken out of the furnace.

Characterization

The steel/GM interface was investigated in order to understand the mechanisms of steel/GM interaction. Sample involving steel/GM interface was embedded in

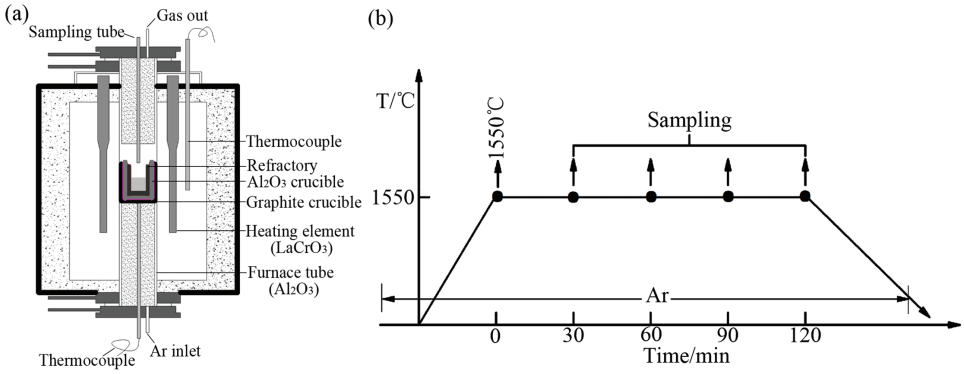

Figure 1: (a) Experimental set-up and (b) Experimental procedure scheme.

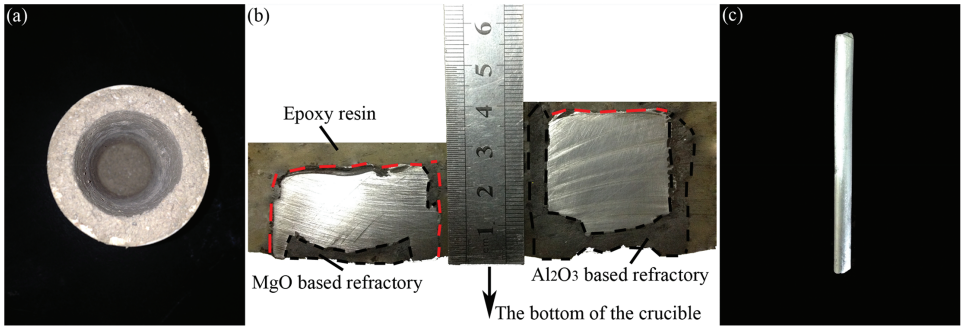

Figure 2: (a) The alumina crucible coated with a lay of gunning material, (b) The steel/refractory interface embedded in an epoxy resin, (c) The obtained steel sample.

an epoxy resin and polished (Figure 2(b)). The microstructure and composition of the specimens were analyzed by a field emission scanning electron microscope (FE-SEM, Model: Nova 400 Nano) with energy dispersive spectrometer (EDS, Model: Le350 PentaFETx-3). The phase change of the refractory was analyzed by means of X-ray diffractometer (XRD, Model: X' Pert pro). The obtained steel sample (Figure 2(c)) was cut into three parts. The first part of the sample was prepared for inclusion characterization. The number and size distribution of inclusions were counted by Image Pro-Plus 6.0 software with photos from 30 randomly visual fields (area: 300 μm × 250 μm) of the SEM at 2000 magnification. The second part of the steel sample was used for the steel composition analysis. Around 0.3 g steel sample was dissolved in HCl acid solution (volume ratio of water with concentrated hydrochloric acid = 1:1) at 353 K (80 °C), the solution was filtered by the membrane filter (0.25 μm). The filtered solution was prepare for Al, Ti, Si, Mn and Mg determination by ICP-AES. The third part of the sample for T. O and total nitrogen (T. N) analysis was ground to remove the rust, then analyzed by Oxygen and Nitrogen Analyzer, in which the T. O content was measured by the inert gas fusion-infrared absorptiometry and the T. N content was determined by inert gas fusion-thermal conductivity method.

Results

Microstructure characterization of the steel/GM interface

The cross section of the samples is presented in Figure 2(b). After 2 h contacting with liquid steel, the remained thickness of MgO GM is thinner than that of Al_2O_3 GM. Figure 3(a) and (c) shows the microstructure of the steel/refractory interface. Lots of fine iron particles (the white dot in Figure 3(a) and (c)) exist in gunning materials near the steel/GM interface because the molten steel infiltrates into the gunning materials. The infiltration layer thickness of Al_2O_3 GM is about 200 μm, however, that of MgO GM is about 1.2 mm. Compared with MgO GM, Al_2O_3 GM exhibits better infiltration resistance to molten steel.

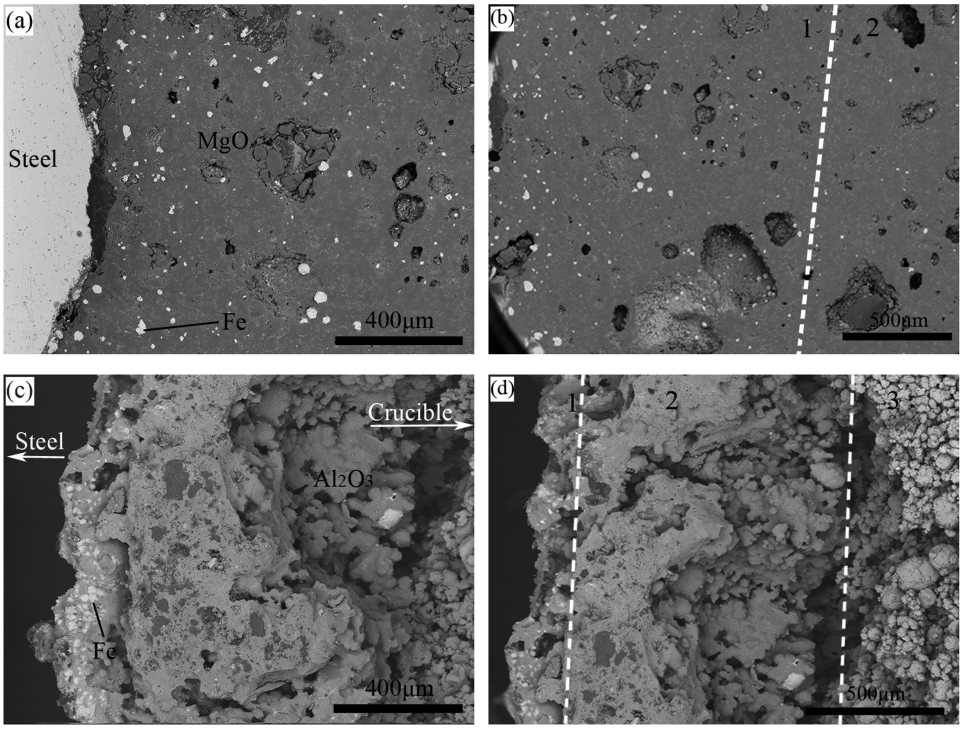

Figure 3: SEM images of (a,c) the steel/GM interface and (b,d) corroded gunning materials : a,b-MgO-based gunning materials with severe infiltration (b-1 infiltrated layer, b-2 original layer); c,d-Al_2O_3-based gunning materials with moderate infiltration (d-1 infiltrated layer, d-2 transition layer, d-3 original layer).

The SEM image of corroded gunning materials is shown in Figure 3(b) and (d). It can be observed that MgO GM has two layers, infiltrated and origin one, Al_2O_3 GM has three layers, infiltrated, transition, and origin one. The region including most of metal is infiltrated layer (b-1, d-1). The grey and dense layer is the transition layer (d-2). The relatively loose layer is the original layer (b-2, d-3). Al_2O_3 GM has a thinner infiltrated layer and the transition layer prevent further infiltration by steel. The cracks between transition layer and original layer in Al_2O_3 GM are formed either by (1) thermal shock during cooling or (2) mechanical load during sample preparation.

The SEM image and EDS elements mapping of corroded MgO and Al_2O_3 GM are shown in Figure 4.

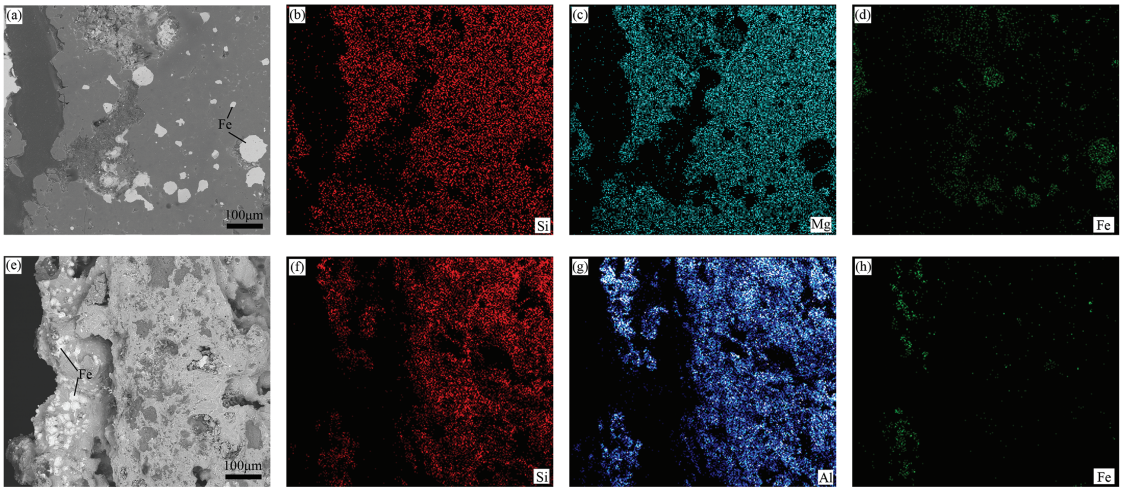

Figure 4: SEM and EDS elements mapping images of corroded MgO (a-d) and Al_2O_3 (e-h)-based gunning materials, (b,f): Si; (c): Mg; (g): Al; (d,h): Fe.

It should be noted: in order to ensure the original morphology of the Al_2O_3 GM and avoid abrasive materials (Al_2O_3 powder) into the pore, the Al_2O_3 GM was not grinded and polished. So the sample of Al_2O_3 GM is not flat, which results in a lower apparent Al concentration in the recessed area, and this is just a false impression. Figure 4(a)–(d) indicates that the steel infiltration damages the integrity of MgO GM. The same phenomenon is found in the Al_2O_3 GM (Figure 4(e)–(h)). The iron particles mainly exist in the surface of the Al_2O_3 GM, whereas the severer and deeper steel infiltration occurs in the MgO GM, resulting in larger iron particles and severer structure damage in the MgO GM. The differences of Mg mapping over the observed region are caused by the steel infiltration and the cracks (formed by thermal shock during cooling or mechanical load during sample preparation) in the GM.

XRD patterns of the refractory

XRD patterns of two types of gunning materials after experiment are presented in Figure 5. The hot face is closed to molten steel. The phase composition of hot face and the original layer after test are nearly the same in the MgO GM (Figure 5(a)). Compared with the original layer, single SiO_2 phase is not found in the hot face of Al_2O_3 GM, this is because the SiO_2 exists in other phases as shown in Figure 5(b). The calculated melting points of Fe_2SiO_4, $CaMgSi_2O_6$, $CaFe_2O_4$ and $CaFeSi_2O_6$ are 1211.1 °C, 1376.6 °C, 1229.7 °C and 1173.1 °C by using the Equilibrium module of the FactSage 6.1, respectively. The database of FToxid was used in the calculation. The low-melting-point phase is existed in both MgO and Al_2O_3 GM.

Compositional evolution of molten steel

The measured results of the steel composition are listed in Table 3. The compositional change of the steel as a function of time is shown in Figure 6, which depicts a clear overview of oxidation sequence for each element in molten steel, that is firstly [Al], followed by the [Ti], [Si], and [Mn]. In both tests, the [Al] content rapidly drops within 30 min, and then stays constant at this level until the completion of the test. A large amount of [Si] pick-up is observed simultaneously with the rapid decrease in [Al] content in the beginning of the test. Afterward the [Si] content slowly decreases or increases in test of MgO and Al_2O_3 GM, respectively. The [Ti] content drops slower in test of Al_2O_3 GM. The [Mn] content decreases slightly in both tests. The Mg content increases in the test of MgO GM, whereas keeps a constant in the test of Al_2O_3 GM. After 2 h holding, the [Al], [Ti], [Mn], [Si] final contents of steel are higher in the test with Al_2O_3 GM.

Table 3: The contents of Al, Ti, Mn and Si in steel samples: I-MgO GM, II-Al_2O_3 GM (10^{-4} mass %).

Sample	Time (min)	Al	Ti	Mn	Si	Mg
Original	0	394	667	770	130	44
I	30	13	17	559	354	158
	60	16	9	479	323	201
	90	12	10	445	326	215
	120	11	9	411	316	258
II	30	32	122	553	2086	53
	60	15	50	559	2330	48
	90	16	27	550	2647	52
	120	16	26	516	2855	48

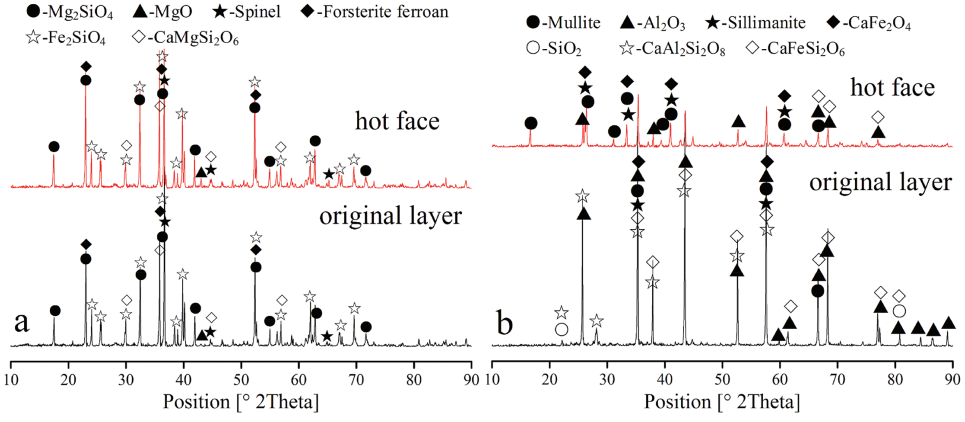

Figure 5: XRD patterns of the hot face and the original layer after experiment: a-MgO-based gunning materials; b-Al_2O_3-based gunning materials.

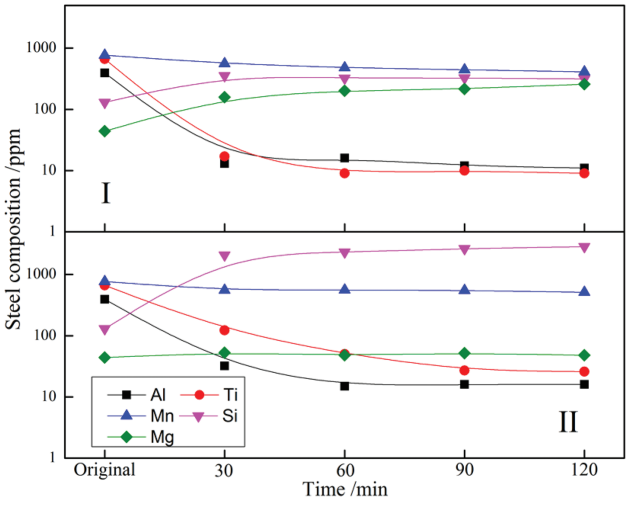

Figure 6: The compositional change of the steel as a function of holding time for different gunning materials: I-MgO-based gunning materials; II-Al_2O_3-based gunning materials.

Figure 7 shows the evolution of the T. O and T. N in the steel as a function of time. The T. O content at 30 min is around 95 ppm using MgO GM, rapidly drops to around 60 ppm and then follows a slow increase until the completion of the test. The T. O content at 30 min is around 120 ppm using Al_2O_3 GM, rapidly drops to around 55 ppm and then follows a slow decrease. After 30 min, the T. O content of steel is lower in test with Al_2O_3 GM. A nitrogen pick-up is observed and similar in both experiments.

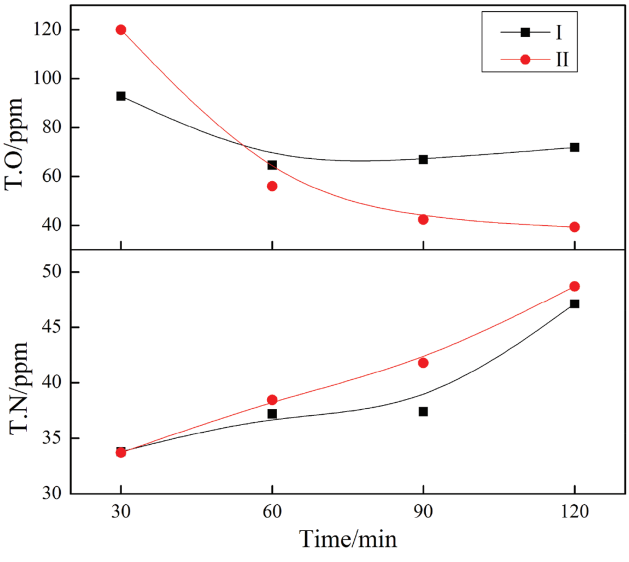

Figure 7: T. O and T. N change of the steel as a function of holding time for different gunning materials: I-MgO-based gunning materials; II-Al_2O_3-based gunning materials.

The number and size distribution of inclusion

Table 4 shows the results of inclusion statistics in steel samples. It should be noted that less than 0.5 μm inclusions were not counted due to the accuracy of the Image Pro-Plus 6.0 software. The inclusion number within 60 min increases from 626 to 777 mm^{-2} in the test of MgO GM, then decreases to 407 mm^{-2} at last. At 30 min, the fraction of inclusions smaller than 1 μm is 49.2 %. At 60 ~ 120 min, the fraction of inclusions smaller than 1 μm increases to 71.7 % ~ 77.2 %, reaches to 76.9 % at last sample. And the average diameter of inclusions decreases from 1.192 μm to 0.923 μm. In order to analyze the distribution of inclusions in detail, the volume fraction of inclusions is calculated by eqs (1)–(3) [20] as follows:

$$Nv = \frac{2}{\pi}\frac{N}{\underline{d}} \tag{1}$$

$$\frac{1}{\underline{d}} = \frac{1}{n}\Sigma\frac{1}{d_i} \tag{2}$$

$$V = \frac{\pi}{6}\frac{\mathrm{d}^3}{}Nv \tag{3}$$

where Nv is the number of inclusions per unit volume in specimen (m^{-3}), N is the number of inclusions per unit area in specimen (m^{-2}), d_i is the apparent size of ith inclusion among n inclusions (m), $\underline{d}$ is the harmonic mean of inclusion size (m) and V represents the volume fraction of inclusions.

As shown in Table 4, the volume fraction of inclusions decreases from 30 min to 120 min in the test of MgO GM. In case of Al_2O_3 GM, the inclusion number increases from 388 to around 461 mm^{-2} within 60 min, then decreases to 239 mm^{-2} at the end. At 30 min, the fraction of inclusions smaller than 1 μm is 46.3 %. At 60 ~ 120 min, the fraction of inclusions smaller than 1 μm increases to 71.8 % ~ 72.0 %, reaches to 72.0 % at last sample. And the average diameter of inclusions decreases from 1.197 μm to 0.964 μm. The volume fraction of inclusions also decreases from 30 min to 120 min. However, compared to the test of MgO GM, the volume fraction of inclusions is lower and the average size of inclusions is larger in the test of Al_2O_3 GM.

The SEM and EDS images of inclusion in steel closed to the steel/GM interface are shown in Figure 8. The large inclusions closed to the steel/refractory interface with irregular shape have a similar composition and structure as the gunning materials, indicating they are the results of gunning materials erosion.

Table 4: The results of inclusion statistics in steel samples taken at different time. The results of inclusion statistics in steel samples taken at different time (I-MgO GM, II-Al_2O_3 GM, *N*- number density of inclusions, *V*-volume fraction of inclusions, *D*-average diameter of inclusions).

No.	Time	*N*	*V*	*D*	Size distribution/%			
	(min)	(mm^{-2})	(10^{-4} %)	(μm)	< 1μm	1 ~ 2μm	2 ~ 3μm	> 3μm
I-1	30	626	1.90	1.192	49.2	42.1	7.1	1.6
I-2	60	777	1.59	0.911	77.2	19.1	3.0	0.7
I-3	90	469	0.97	0.961	71.7	21.6	6.1	0.6
I-4	120	407	0.80	0.923	76.9	18.6	2.6	1.9
II-1	30	388	1.25	1.197	46.3	45.0	5.3	3.4
II-2	60	461	0.95	0.938	71.8	25.4	1.7	1.1
II-3	90	263	0.55	0.995	71.4	19.8	6.9	1.9
II-4	120	239	0.54	0.964	72.0	23.1	4.2	0.7

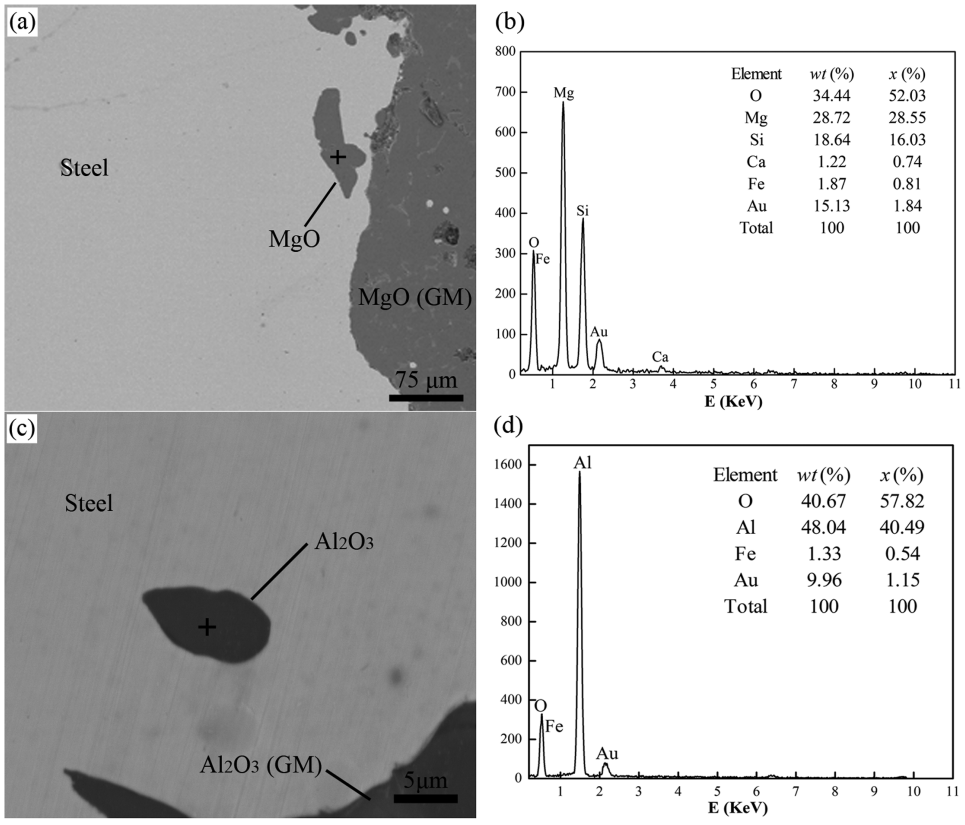

Figure 8: The (a,c) SEM and (b,d) EDS images of inclusion in steel closed to the steel/GM interface after the test: (a,b)- MgO GM, (c,d)- Al_2O_3 GM.

Discussion

The steel/GM interface

MgO GM has two layers, infiltrated and original layer; Al_2O_3 GM has three layers, infiltrated, transition and original layer. The infiltrated layer is thinner in the case of Al_2O_3-based gunning materials. The iron particles mainly exist in the infiltration layer due to the existence of transition layer (Figure 3). The compositional evolution of steel (Figure 6) implies that SiO_2 and Fe_2O_3 in gunning materials are reduced by the dissolved Al, Ti, Mn and Si in molten steel (eqs (4)–(6)).

$$4[Al] + 3SiO_2 \rightarrow 3[Si] + 2Al_2O_3 \quad (4)$$

$$[\mathrm{Ti}] + \mathrm{SiO_2} \rightarrow [\mathrm{Si}] + \mathrm{TiO_X} \quad (5)$$

$$[\mathrm{Al, Ti, Si, Mn}] + \mathrm{Fe_2O_3} \rightarrow \mathrm{Fe} + (\mathrm{Al, Ti, Si, Mn})\mathrm{O_Y} \quad (6)$$

According to the above experimental results, the schematic illustration of corrosion mechanism of gunning materials is shown in Figure 9. [M] denotes deoxidizing elements in steel such as [Al], [Ti], [Mn] and [Si]; S denotes reducible oxides in gunning materials such as SiO_2 and Fe_2O_3. A donates insoluble materials in gunning materials such as MgO, Al_2O_3 and so on; L denotes pores and low melting point phases such as Fe_2SiO_4, $CaMgSi_2O_6$, $CaFe_2O_4$, $CaFeSi_2O_6$ (Figure 5); I and MP, respectively means inclusions formed by the interaction and the metal particles in gunning materials. The steel infiltration may involve several elemental steps as shown in (Figure 9(a)–(d)). (a) Molten steel contacts with gunning materials, but doesn't start to react. (b) SiO_2 and Fe_2O_3 in the surface of gunning materials are reduced by the dissolved Al, Ti, Mn and Si in molten steel, leading to formation of the inclusions in steel; oxides with lower melting point may flow into molten steel, spaces remained will be infiltrated by molten steel, iron formed by Fe_2O_3 then stays there in its origin position. It agrees well with the results of Figure 4, the content of SiO_2 is lower in the infiltration layer. Moreover, the pores and low-melting-point phase oxides become the passageway for steel infiltration. (c) Further steel infiltration damages the integrity of gunning materials at high temperature, the structure of gunning materials becomes loose (Figure 4), and lots of inclusions are formed. (d) Particles of GM falls into molten steel to form the large inclusion due to the structure damage of the gunning materials, these large inclusions have a similar composition as the gunning materials as confirmed by Figure 8.

The low melting point phase and molten steel flow into the interparticle pores and subsequently penetrate into the compact particle boundaries [4]. Finally, the high melting point particles (Al_2O_3) are surrounded by the liquid phase and dissolved into the molten oxide mixture at high temperature, resulting in a higher viscosity and worse fluidity in the molten oxide mixture. With more particles dissolved into the oxide mixture, the liquid phase becomes more viscous to blocking the pores [15]. This is the formation mechanism of the dense transition layer, which slows down the material transfer in gunning materials and prevents further steel infiltration. Compared with MgO GM, the contact angle between

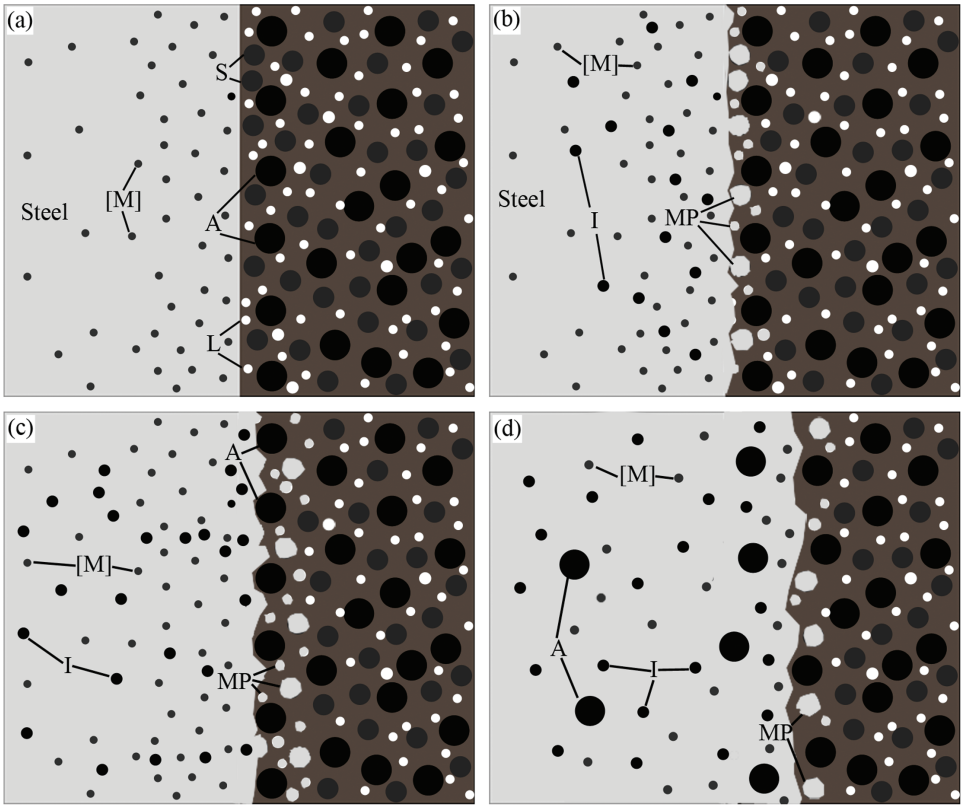

Figure 9: Schematic representations of GM infiltrated by steel.

molten steel and Al_2O_3 GM is larger ($\theta Al_2O_3/Fe > 140°$) [21, 22]. Therefore, the Al_2O_3 GM is found to be less prone to steel penetration due to its poor wetting and the dense transition layer. The lager iron particles and severer structure damage occurs in the MgO GM (Figure 4). The refractory materials particle drops into liquid steel, resulting in an increase in Mg content in test of MgO. The residual thickness of MgO GM is thinner than that of Al_2O_3 GM after 2 h high temperature holding experiments (Figure 2).

Oxidizing capacity of gunning materials

During the interaction between steel and gunning materials, the dissolved Al and Ti in steel have priority in deoxidizing due to their stronger ability to combine with oxygen, [Si] content increases accordingly. The compositional evolution of steel (Figure 6) implies that (a) SiO_2 in gunning materials is reduced by [Al] and [Ti] in molten steel, leading to the reoxidation of steel; (b) with the further interaction, the dissolved Si and Mn also starts to be oxidized as [Al] and [Ti] have been depleted and (c) the extent of steel reoxidation varies with the type of gunning materials, thus, less reoxidation occurs with the Al_2O_3 GM. It is clear that [Al], [Ti], and [Mn] reacts with oxygen supplied from the gunning materials, resulting in steel reoxidation. The oxidation capacity of gunning materials can therefore be quantified by the amount of the oxygen supplied from gunning materials to molten steel (O_R) during the interaction, which can be calculated as eq. (7) [8].

$$O_R = \sum \left([M]_{initial} - [M]_{final} \right) \frac{yW_O}{xW_M} \tag{7}$$

where M represents dissolved Al, Ti, and Mn in molten steel; W_O and W_M is the atomic weight of oxygen and M, respectively; and x and y is the atom numbers of M and O in the stable oxide M_xO_y. It should be noted that the evolution of Si is not considered in eq. (7) because (a) [Si] would be the product of the reoxidation reaction and (b) due to the inaccuracy of the [Si] analysis [8].

O_R can be calculated according to the data in the Table 3. Figure 10 shows the evolution of oxygen quantity supplied from the gunning materials to molten steel. The MgO GM supplies more oxygen (about 900 ppm at end of the experiment) than Al_2O_3 GM (about 800 ppm), showing a stronger oxidizing capacity of MgO GM due to its higher reducible component (10.5 wt.% SiO_2 + 2 wt. % Fe_2O_3). It should be noticed that in the present tests the amount of gunning materials compared with that of steel is large, providing extreme compositional exchange capacity with respect to the steel. For both tests, the supplied oxygen rapidly increases in the first 30 min and then levels off, indicating that the steel oxidation is much severer at the beginning of the interaction. This is because (1) a large contact interface provides enough site for steel reoxidation in the beginning of test and consequently leads to a strong steel reoxidation (step 1), (2) with the depletion of [Al] and [Ti], i. e., elements that are prone to be oxidized, the driving force for steel reoxidation decreases and consequently the speed for steel reoxidation decreases as well, (3) the steel (with high [Al] and [Ti] content) and oxygen have to reach the reaction layer to continue the reoxidation reaction once the SiO_2 and Fe_2O_3 are depleted at the original steel/refractory interface (Step 2) [8]. Compared with chemical reaction (step 1) at the original steel/refractory interface, step 2 is much slower since it is mainly determined by the temperature, porosity and/or oxygen diffusivity. The porosity influences the steel infiltration speed into the gunning materials. With the interaction going on, the contents of [Al] and [Ti] decrease, the concentration gradient of [Al] and [Ti] decreases, so the mass transfer becomes slower. As a result, much severer steel reoxidation takes place in the beginning and a slower reoxidation rate follows.

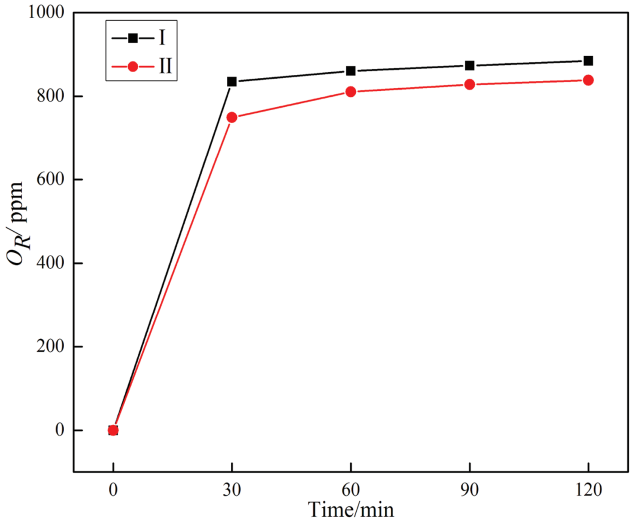

Figure 10: Evolution of oxygen quantity supplied from the gunning materials to molten steel as a function of time: I-MgO GM, II-Al_2O_3 GM.

The T. O in steel samples consists of two parts: (a) oxygen from the inclusion in steel and (b) the

dissolved oxygen in steel. Dissolved oxygen can be calculated according to thermodynamic equilibrium by eqs (8 [21], 9 and 10).

$$2[\mathrm{Al}] + 3[\mathrm{O}] = \mathrm{Al_2O_3(s)}, \lg K_{\mathrm{Al}} = \frac{63655}{T} - 20.58 \tag{8}$$

$$1/K_{\mathrm{Al}} = \{f_{\mathrm{Al}} w[\mathrm{Al}]\}^2 \{f_{\mathrm{O}} w[\mathrm{O}]\}^3 \tag{9}$$

$$\begin{aligned} \lg f_{\mathrm{Al}} = {} & e_{\mathrm{Al}}^{\mathrm{Al}} w[\mathrm{Al}] + e_{\mathrm{Al}}^{\mathrm{C}} w[\mathrm{C}] + e_{\mathrm{Al}}^{\mathrm{Si}} w[\mathrm{Si}] \\ & + e_{\mathrm{Al}}^{\mathrm{S}} w[\mathrm{S}] + e_{\mathrm{Al}}^{\mathrm{Ti}} w[\mathrm{Ti}] + e_{\mathrm{Al}}^{\mathrm{N}} w[\mathrm{N}] \end{aligned} \tag{10}$$

$$e_{\mathrm{B(T)}}^{\mathrm{K}} = \left(\frac{2538}{T} - 0.355\right) e_{\mathrm{B(1873)}}^{\mathrm{K}} \tag{11}$$

f_{Al} can be calculated according to Table 5 and eq. (11) [20], $f_{\mathrm{O}} \approx 1$. The content of dissolved oxygen is 12 ~ 15.5 ppm in test of MgO GM and 7.6 ~ 12 ppm for Al_2O_3 GM. This shows that the most of the oxygen is from inclusions in steel. Comparison of measured TO content of sample and calculated O_R is shown in Figure 11. The quantity of oxygen supplied from the gunning materials to the molten steel is much larger than the measured T. O content. This arises from (1) the floatation of the oxidation products. Non-metallic inclusions have a relatively smaller density compared to the molten steel, and therefore floats to the top surface of the molten steel, decreasing the T. O; (2) steel infiltration, i. e., part of the molten steel is reoxidized inside the gunning materials. The formed nonmetallic inclusions are therefore entrapped inside the gunning materials and would not contribute to the T. O significantly in steel phase.

Table 5: Activity interaction parameters of elements in steel [21].

e_i^j	Al	C	Si	S	Ti	N
Al	0.045	0.091	0.0056	0.035	0.016	−0.053

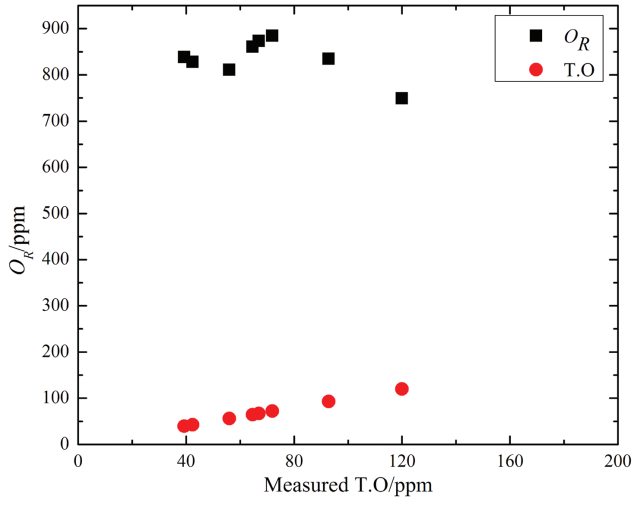

Figure 11: Comparison of measured TO content of sample and calculated O_R.

Effects on the steel cleanliness

Firstly, it can be seen from the above results that O_R (Figure 10) increases with the interaction time for all the experiments, indicating a continuous steel reoxidation. Secondly, considerably lower values of the number density, volume fraction of inclusions (Table 4) and T. O contents (Figure 7) are observed in the test with Al_2O_3 GM, pointing out that the Al_2O_3 GM provides a less reactive condition. Plenty of smaller inclusions are found in test with MgO GM (Table 4). Magnesia formed by magnesium deoxidation in liquid steel grows slowly [23], so the size of MgO inclusions is smaller. Fewer inclusions with relatively larger size are found in the steel in test of Al_2O_3 GM. This relatively larger inclusion could result from refractory and the agglomeration of Al_2O_3 inclusions [2]. After 30 min, the fraction of inclusions smaller than 1 μm becomes larger because the larger inclusions easily float up to the top of liquid steel. Furthermore, it has been mentioned in Section 4.2 that the interaction between liquid steel and GM becomes slower after 30 min. The inclusions formed by deoxidization and shedding of GM become less and less.

The T. O content decreases (Figure 7), the inclusion number density (Table 4) and the size of inclusions decreases, indicating that most of new inclusions have small size, and part of large-size inclusions floats to the surface of molten steel. So the steel reoxidation slightly increases the T. O content in steel, indicating that the main fraction of the reoxidation products don't stay in steel phase. These analyses agree well with the T. O < O_R. The use of Al_2O_3 GM results in an improved steel cleanliness because the transition layer in Al_2O_3 GM slows down the mass transfer and the Al_2O_3 GM contains lower reducible oxides.

Conclusions

The interaction between steel and gunning materials used in tundish was investigated at 1823 K on laboratory scale. The phase change and erosion of refractory was studied. The steel cleanliness by using distinct gunning materials, namely, MgO and Al_2O_3 GM was compared. The compositional evolution of molten steel was analyzed. The main results are summarized as follow:

(1) SiO_2 and Fe_2O_3 in gunning materials are reduced by the dissolved Al, Ti, Mn and Si in molten steel, and then liquid steel penetrates into the sites where they locate, resulting in steel infiltration. The pores and low melting point phases in gunning materials also provide the passageway for steel infiltration. The steel infiltration damages the integrity of gunning materials, as a result, the refractory materials particles fall into liquid steel to become large-sized inclusions.
(2) The Al_2O_3 GM is found to be less prone to steel penetration due to its poor wetting with molten steel and the dense transition layer. However, the much severer steel infiltration occurs in test of MgO GM because of its better wetting properties.
(3) The molten steel is quickly oxidized by gunning materials in beginning of the interaction. Almost all of the [Al] are consumed within 30 min of contacting with gunning materials. A large amount of [Si] pick-up is observed simultaneously with the rapid change in [Al] content, which implies that SiO_2 in refractory is reduced.
(4) The oxidation capacity of gunning materials highly depends on their chemical composition. MgO GM with higher reducible content (10.5 wt.% SiO_2 + 2 wt. % Fe_2O_3) has a stronger oxidation capacity than Al_2O_3 GM. The quantity of oxygen supplied from the gunning materials to molten steel is much larger than the measured T. O content due to the floatation of inclusions.
(5) Al_2O_3 GM could be a promising GM in the tundish due to less contamination into the molten steel.

Funding: The authors wish to express their appreciation to the Major State Basic Research Development Program of China (Grant No. 2014CB660800) for providing financial support which enabled this study to be carried out.

References

[1] J.W. Lee and J.G. Duh, J. Mater. Res., 18 (2003) 1950–1959.
[2] P. Yan, M.-A. Van Ende, E. Zinngrebe, S. van der Laan, B. Blanpain and M. Guo, ISIJ Int., 54 (2014) 2551–2558.
[3] S. Jansson, V. Brabie and P. Jönsson, Ironmak. Steelmak., 33 (2006) 389–397.
[4] Y. Wei, N. Li and C. Ke, Am. Ceram. Soc. Bull., 86 (2007) 9201–9205.
[5] G. Cornacchia, M. Gelfi, C. Mapelli, A. Paderni, S. Panza and R. Roberti, ISIJ Int., 47 (2007) 392–401.
[6] A. Kumar, V. Thapliyal, D.G. Robertson and J.D. Smith, J. Am. Ceram. Soc., 98 (2015) 1596–1603.
[7] R. Khanna, M.I.U. Haq, Y. Wang, S. Seetharaman and V. Sahajwalla, Metall. Mater. Trans. B., 42 (2011) 677–684.
[8] P. Yan, S. Arnout, M.-A. Van Ende, E. Zinngrebe, T. Jones, B. Blanpain and M. Guo, Metall. Mater. Trans. B., 46 (2015) 1242–1251.
[9] M. Mantovani, L. Moraes, Jr, R. Leandro da Silva, E. Cabral, E. Possente, C. Barbosa and B. Ramos, Ironmak. Steelmak., 40 (2013) 319–325.
[10] K. Sasai and Y. Mizukami, ISIJ Int., 40 (2000) 40–47.
[11] J. Lehmann, M. Boher and M. Kaerle, Cim. Bull., 90 (1997) 69–74.
[12] J.-H. Son, I.-H. Jung, S.-M. Jung, H. Gaye and H.-G. Lee, ISIJ Int., 50 (2010) 1422–1430.
[13] L. Chen, A. Malfliet, P.T. Jones, B. Blanpain and M. Guo, Ceram. Int., 42 (2016) 743–751.
[14] A. Luz, F. Leite, M. Brito and V. Pandolfelli, Ceram. Int., 39 (2013) 7507–7515.
[15] L. Scheunis, A.F. Mehrjardi, M. Campforts, P.T. Jones, B. Blanpain and E. Jak, J. Eur. Ceram. Soc., 34 (2014) 1599–1610.
[16] S. Zhang, H. Sarpoolaky, N. Marriott and W. Lee, Br. Ceram. Trans., 99 (2000) 248–255.
[17] R. Kaur, D. Swinbourne, M. Wadsley and C. Nexhip, Metall. Mater. Trans. B., 42 (2011) 451–459.
[18] H.B. Kim and M.S. Oh, Ceram. Int., 34 (2008) 2107–2116.
[19] R. Puente-Ornelas, C. Lizcano-Zulaica, A. Guzmán, P. Zambrano and T. Das-Roy, Fuel, 93 (2012) 581–588.
[20] H. Goto, K. Miyazawa and K. Tanaka, ISIJ Int., 35 (1995) 286–291.
[21] X.H. Huang, Theory of Iron and Steel Metallurgy, 3rd ed., Metallurgical Industry Press, Beijing (2012), pp. 223–396.
[22] D. Poirier, H. Yin, M. Suzuki and T. Emi, ISIJ Int., 38 (1998) 229–238.
[23] H. Ohta and H. Suito, ISIJ Int., 46 (2006) 22–28.